ACTA ABP BIOCHIMICA POLONICA

Vol. 70, No 3/2023
509–516
https://doi.org/10.18388/abp.2020_6404

Regular paper

Downregulation of circular RNA 00091761 protects against heart failure after myocardial infarction *via* microRNA-335-3p/ ASCL4 axis

Qian Wei[1#], Mengni Jiang[2#], Bin Tang[1], Lanlan You[1] and Lin Zhao[1]✉

[1]Department of Ultrasonics Medicine, Chengdu Medical College, Clinical Medical College and The First Affiliated Hospital of Chengdu Medical College, Sichuan 610500 China; [2]Department of Cardiovascular Medicine, Chengdu Medical College, Clinical Medical College and The First Affiliated Hospital of Chengdu Medical College, Sichuan 610500 China

Our research tended to explore the biological roles and expression status of circ_00091761 in HF after MI. The hypoxia reoxygenation (H/R) injured H9c2 cells model was constructed to simulate HF after MI. The expression of circ_0091761 was examined in H/R injured H9c2 cells by qRT-PCR. Then, the effect of circ_0091761 expression on the proliferation of H/R injured H9c2 cells was evaluated by CCK-8 along with TUNEL assay. Secretion of lactate dehydrogenase (LDH), reactive oxygen species (ROS), Fe^{2+}, glutathione (GSH), and malondialdehyde (MDA) was measured to evaluate cell ferroptosis of H/R injured H9c2 cells, along with protein levels of glutathione peroxidase 4 (GPX4), solute carrier family 7 member 11 (SLC7A11), and transferrin receptor protein (TFRC). Luciferase reporter as well as RNA pull-down assays revealed the binding relationship between miR-335-3p and circ_0091761 or ASCL4. Circ_0091761 was upregulated in H/R injured H9c2 cells. Knockdown of circ_0091761 promoted cell proliferation and suppressed ferroptosis of H/R injured H9c2 cells. Interestingly, circ_0091761 sponges miR-335-3p to upregulate acyl-CoA synthetase long-chain family member 4 (ACSL4) expression. miR-335-3p inhibitor attenuated the effects of circ_0091761 knockdown on cell proliferation and ferroptosis in H/R injured H9c2 cells. Additionally, upregulated ACSL4 abrogated elevated miR-335-3p-induced effects on H/R injured H9c2 cells. Circ_0091761 inhibited cell proliferation and accelerated ferroptosis of H/R injured H9c2 cells by sponging miR-335-3p to upregulated TFRC axis. Therefore, Inhibition of circ_0091761 may protect against HF after MI.

Keywords: heart failure, myocardial infarction, circ_0091761, miR-335-3p, ASCL4

Received: 23 June, 2022; revised: 30 December, 2022; accepted: 01 February, 2023; available on-line: 06 September, 2023

✉e-mail: drzhaolin@hotmail.com
#These authors contributed equally to this work and should be considered co-first authors.

Abbreviations: ACSL4, acyl-CoA synthetase long-chain family member 4; CCK-8, Cell Counting Kit-8; circRNA, circular RNA; DCFH-DA, 2′,7′-Dichlorodihydrofluorescein diacetate; DMEM, dulbecco's modification of eagle's medium; ECL, enhanced chemiluminescence; Fer-1, ferrostatin-1; GPX4, glutathione peroxidase 4; GSH, glutathione; H/R, hypoxia reoxygenation; HF, heart failure; LDH, lactate dehydrogenase; MDA, malondialdehyde ; MI, myocardial infarction; miRNA, micro RNA; NC, negative control; OE, overexpression; PVDF, polyvinylidenefluoride; qRT-PCR, quantitative real time polymerase chain reaction; ROS, reactive oxygen species; SD, standard deviation; SLC7A11, solute carrier family 7 member 11; TFR1, transferrin receptor protein; TUNEL, TdT-mediated dUTP nick end labeling

INTRODUCTION

Heart failure (HF) is an acute decompensation of cardiac function under various causes. The etiology and inducement of HF are complex and diverse. The necrosis of myocardial cells caused by acute ischemia and hypoxia of the coronary artery during myocardial infarction (MI) is the main cause of HF and also one of the common causes of acute decompensation of HF (Bahit *et al*., 2018; Orrem *et al*., 2018). HF after MI seriously endangers the life and health of patients. Early accurate judgment will greatly benefit the treatment and prognosis of the disease.

In recent years, a new type of programmed death, named ferroptosis, is found to play an essential role in diverse disorders (Xie *et al*., 2016). Because of the dysfunction of oxidative metabolism of the cell membrane phospholipids, biofilm polyunsaturated fatty acids (PUFAs) lipid peroxidation occurs reduced glutathione (GSH) in cells will not be able to return the excess of harmful lipid hydroperoxide as harmless fatty alcohols, free iron ion mediated Fenton reaction catalyzed the accumulation of lipid free radicals within the cell leads to cell ferroptosis (Cao & Dixon, 2016). Accumulated evidence demonstrates that ferroptosis participates in HF after MI (Hu *et al*., 2021). However, the specific mechanism needs to be further researched to clarify.

Circular RNAs (circRNAs) are a class of non-coding RNAs (ncRNAs) which can regulate the expression of several key genes by combining with microRNAs (miRNAs) or other molecules (Meng *et al*., 2017; Ashwal-Fluss *et al*., 2014; Zhang *et al*., 2017). Most circRNAs show miRNA binding capabilities, and are identified as miRNA sponges and enhance downstream gene expression by sponging miRNA (Li *et al*., 2019). Recently, researchers found the significance of circRNAs in regulating cell functions and disease processes (Meng *et al*., 2017; Ashwal-Fluss *et al*., 2014; Zhang *et al*., 2017). Furthermore, growing evidence shows that circRNA has the potential to become a promising biomarker for diagnosis and therapeutic targets of HF after MI (Devaux *et al*., 2017; Altesha *et al*., 2019). For instance, through the ceRNA mechanism, the circHipk3 accelerates cardiac regeneration after MI via the miR-133a-CTGF axis (Si *et al*., 2020).

CircRNA_0001654, circRNA_0091761, circRNA_0405624, and circRNA_0406698 have been identified to be obviously upregulated in MI (Zhao *et al*., 2020)., and circRNA_0091761 expressions were demonstrated to be the most significant difference in H/R injured H9c2 cells.

Therefore, this study aimed to further explore the specific mechanism of circRNA_0091761 in HF after MI *in vitro*.

MATERIALS AND METHODS

Materials

H9c2 rat cardiomyoblast cell line (American Type Culture Collection, USA). Primary antibodies and internal reference protein (Abcam Company, USA): anti-GPX4 (ab125066, 1: 1000), anti-SLC7A11 (ab175186, 1: 3000), and anti-TFR1 (ab214039, 1: 1000). anti-GAPDH (ab8245,1: 1000). HRP labeled anti-rabbit secondary antibody (Beyotime Biotech, China). Plasmids for cell transfection (Gibco, USA): si-circ_0091761 1#, si-circ_0091761 2#, miR-335-3p mimic, miR-335-3p inhibitor, oe-ACL4, and their negative controls. Polybrene and purinomycin (Sigma, USA). Lipofectamine 3000 and the reverse transcription kit (Invitrogen, USA). Fetal bovine serum (FBS; Biological Industries, USA). PrimeScript™ RT-PCR Kit (Vazyme Biotech, China). TRIzol reagent (Invitrogen, USA), Nanodrop 2000 spectrophotometer (Mettler Toledo, China). RIPA lysate (Beyotime, China). Primer sequences for circ_0091761, miR-335-3p, and all mRNAs were designed by RiboBio (Guangzhou, China). RNase R treatment (Genesee, Guangzhou, China). miRNeasy Mini Kit (QIAGEN, Dusseldorf, Germany). Actinomycin D (Merk, USA). SuperScript First-Strand Synthesis Kit (Invitrogen, USA). LDH Cytotoxicity Assay Kit (Beyotime, China). Spectrophotometer (Thermo Fisher, USA). Oxidation-sensitive fluorescent probe DCFH-DA (Sigma, USA). Iron Assay Kit (ab83366, Abcam, USA). Glutathione Assay Kit (CS0260; Sigma, USA). Malondialdehyde Kit (ab118970, Abcam, USA). Cell counting kit 8 (CCK-8; Beyotime, China). TUNEL detection kit (ab66110, Abcam, USA). Microscope (Nikon, Japan). BCA kit (Sigma, USA). PVDF membranes (Bio-Rad, USA). Dual-Luciferase Reporter Assay kit (K801-200; BioVision Tech, San Francisco, USA). Pierce™ Magnetic RNA-Protein Pull-Down Kit (Thermo Fisher, Waltham, MA, USA).

Cell culture

H9c2 cells were cultured using a DMEM medium containing 10% FBS and 1% penicillin/streptomycin, and placed in an incubator (5% CO_2, 37°C). Then, the hypoxia-reoxygenation (H/R) injured H9c2 cells model was conducted to mimic HF after MI. H9c2 cells were incubated in a hypoxic environment (95% N_2 and 5% CO_2) at 37°C for 3 h. Then, DMEM free of FBS was added to H9c2 cells in a standard incubator for 4 h.

qRT-PCR

qRT-PCR was performed to measure the mRNA levels of circRNA_0001654, circRNA_0091761, circRNA_0405624, circRNA_0406698, miR-335-3p, and ACSL4. Firstly, TRIzol was used to isolate RNA of H/R injured H9c2 cells, and RNA concentration was analyzed using a spectrophotometer. M-MLV was used to synthesize cDNA through reverse transcription. qRT-PCR was conducted with the PrimeScript™ RT-PCR Kit. GAPDH and U6 were used as reference genes. Relative gene expression was calculated through the $2^{-\Delta\Delta Ct}$ method.

Stability detection of circular RNA

RNase R treatment is mainly used for circRNA identification and stability detection (Xiao MS & Wilusz JE, 2019). 5 μg total RNA extracted from H/R injured H9c2 cells were digested by RNase R enzyme. The circRNA_0091761 and the linear type mRNA levels were detected by qRT-PCR with 2 μg/mL actinomycin D for 0, 4, 8, 12, and 24 h.

Detection of lactate dehydrogenase (LDH) activity

H9c2 cells were seeded in 96-well plates and cultured in a medium containing LDH reagent for 0.5 h to measure LDH release according to the LDH kit procedure, which was provided by Nanjing Jiangcheng Bioengineering Institute (Nanjing, China).

Detection of reactive oxygen species (ROS) activity

H9c2 cells were treated with DCFH-DA (10 μmol/L) for 0.5 h at 37°C. Then, the fluorescence intensity of each group was detected under a fluorescence microscope (488 nm excitation wavelength, 525 nm emission wavelength).

Detection of Fe^{2+} content

After H9c2 cells were lysed, the Fe^{2+} level of cells in each group was detected according to the procedure of the Fe^{2+} detection kit, which was provided by Nanjing Jiangcheng Bioengineering Institute (Nanjing, China).

Detection of glutathione (GSH)content

After H9c2 cells were lysed, the GSH level of cells in each group was detected according to the procedure of the GSH Assay Kit, which was provided by Nanjing Jiangcheng Bioengineering Institute (Nanjing, China).

Detection of malondialdehyde (MDA)

After H9c2 cells were lysed, the MDA level of cells in each group was detected according to the procedure of the MDA Kit, which was provided by Nanjing Jiangcheng Bioengineering Institute (Nanjing, China).

Cell viability assay

Cell counting kit 8 (Beyotime, Shanghai, China) has been used to evaluate the cell viability of $H9C_2$ cells of each group. Cells were collected and seeded into a 96-well plate after successful transfection. Afterwards, cell viability was detected using a microplate under the absorbance of 450 nm after a supplement of CCK-8 reagents.

TUNEL assay

H9c2 cell death was measured by a TUNEL detection kit according to the instructions of the manual (Beyotime). The H/R injured H9c2 cells were observed under a microscope.

Western blotting assay

Ferroptosis-related proteins including glutathione peroxidase 4 (GPX4), solute carrier family 7 member 11 (SLC7A11), and transferrin receptor protein (TFRC) were measured in H9c2 cells of each group. Total protein was extracted from the H9c2 cells by RIPA buffer, and determined with the BCA kit. Subsequently, proteins were isolated with 12% SDS-PAGE gel and were moved onto PVDF membranes. Then the membranes were blocked with 5% defatted milk for 2 h and then incubated with primary antibodies overnight at 4°C. Immune complexes were then incubated with secondary antibody. Finally, the ECL chemiluminescence method was used to detect the expression of each protein. All experiments were repeated three times.

Dual-luciferase reporter assay

According to the reported methods, circRNA_0091761 as well as ACSL4 recombinant pyratinase reporter plasmids containing the binding sequence of miR-335-3p and regroup plasmids containing the abrupt change of binding sequence were constructed. H9c2 cells (1×10^5/well) seeded in a 12-well plate were transfected with 1.5 μg recombinant luciferase reporter plasmid, 100 nmol/L miR-335-3p mimic and 10 ng PRL-TK (internal reference plasmid) for 24 h, the intensity of firefly luciferin and renal luciferin were measured.

RNA pull-down assay

500 μg streptavidin magnetic beads combined with a 200 pmol biotin labeled miR-335-3p mimic were added to the RNA extracted from the H9c2 cells. The complexes were gently mixed at room temperature and incubated for 30 min. After eluting buffer was added, the pulled RNA complex was then collected. The circRNA_0091761 and ASCL4 level was quantitatively analyzed by qRT-PCR.

Statistical analysis

Data were analyzed with GraphPad Prism version 8.3 and presented as mean ± SD. Student's t-test (two groups), as well as one-way ANOVA (multiple groups), were applied for difference analysis. A *P* value less than 0.05 was deemed statistically significant.

RESULTS

Circ_0091761 is highly expressed in H/R injured H9c2 cells

Expression of 4 circRNAs which have been identified to be highly expressed in MI was detected in H/R injured H9c2 cells, among which circ_0091761 was obviously highly expressed (Fig. 1A). The results of RNase R treatment indicated that the expression level of the linear group was substantially lower than that in circ_0091761 group (Fig. 1B). Meanwhile, circ_0091761 showed more stable mRNA expression compared with a linear group (Fig. 1C). The level of GSH in H/R injured and RSL3 treated H9c2 cells was notably decreased and increased in Ferrostatin-1 group; however, LDH, ROS, Fe^{2+}, as well as MDA levels were notably elevated by H/R injury and RSL3 and reduced by Ferrostatin-1 (Fig. 1D–I).

Inhibition of circ_0091761 promotes cell viability and inhibited ferroptosis of H/R injured H9c2 cells.

The expression of circ_0091761 was decreased after small interference RNA was transfected into H/R injured H9c2 cells. Circ_0091761 declined more significantly in group si-circ_0091761 1#, which was used in subsequent experiments (Fig. 2A). Knockdown of circ_0091761 notably improved cell viability (Fig. 2B), and suppressed

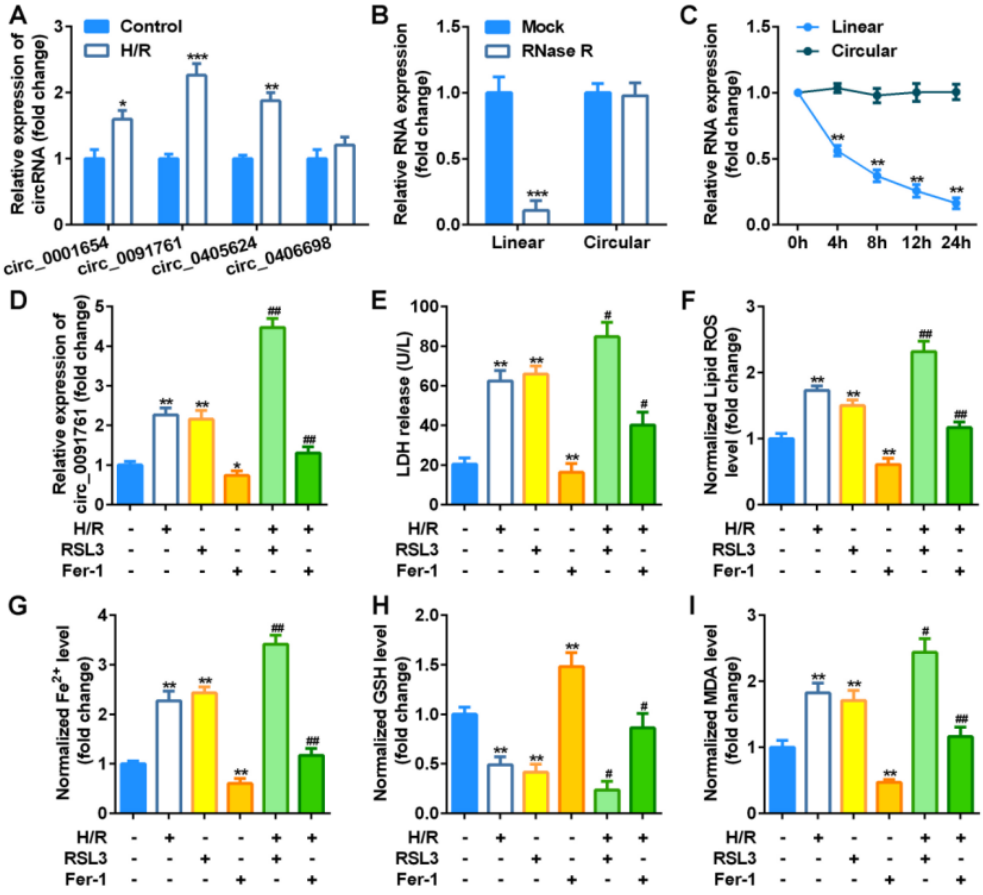

Figure 1. Expression levels of circ_0091761 in H/R injured H9c2 cells.
(**A**) The expression of 4 circRNAs in H/R injured H9c2 cells measured by qRT-PCR, $^{*}p<0.05$, $^{**}p<0.01$, $^{***}p<0.001$. (**B**) qRT-PCR analyses for the expression of circ_0091761 and linear one in H/R injured H9c2 cells after RNaseR treatment, $^{***}p<0.001$. (**C**) qRT-PCR analyses for the expression of circ_0091761 and linear one in H/R injured H9c2 cells at the indicated time after treatment with Actinomycin D, $^{**}p<0.01$. (**D**) The expression of circ_0091761 in H/R injured H9c2 cells measured by qRT-PCR, $^{*}p<0.05$, $^{**}p<0.01$, compared with the control group; $^{\#\#}p<0.01$, compared with the H/R group. (**E**) The LDH, (**F**) ROS, (**G**) Fe^{2+}, (**H**) GSH, and (**I**) MDA levels in H/R injured and RSL3 treated H9c2 cells, $^{**}p<0.01$, compared with the control group; $^{\#}p<0.05$, $^{\#\#}p<0.01$, compared with the H/R group.

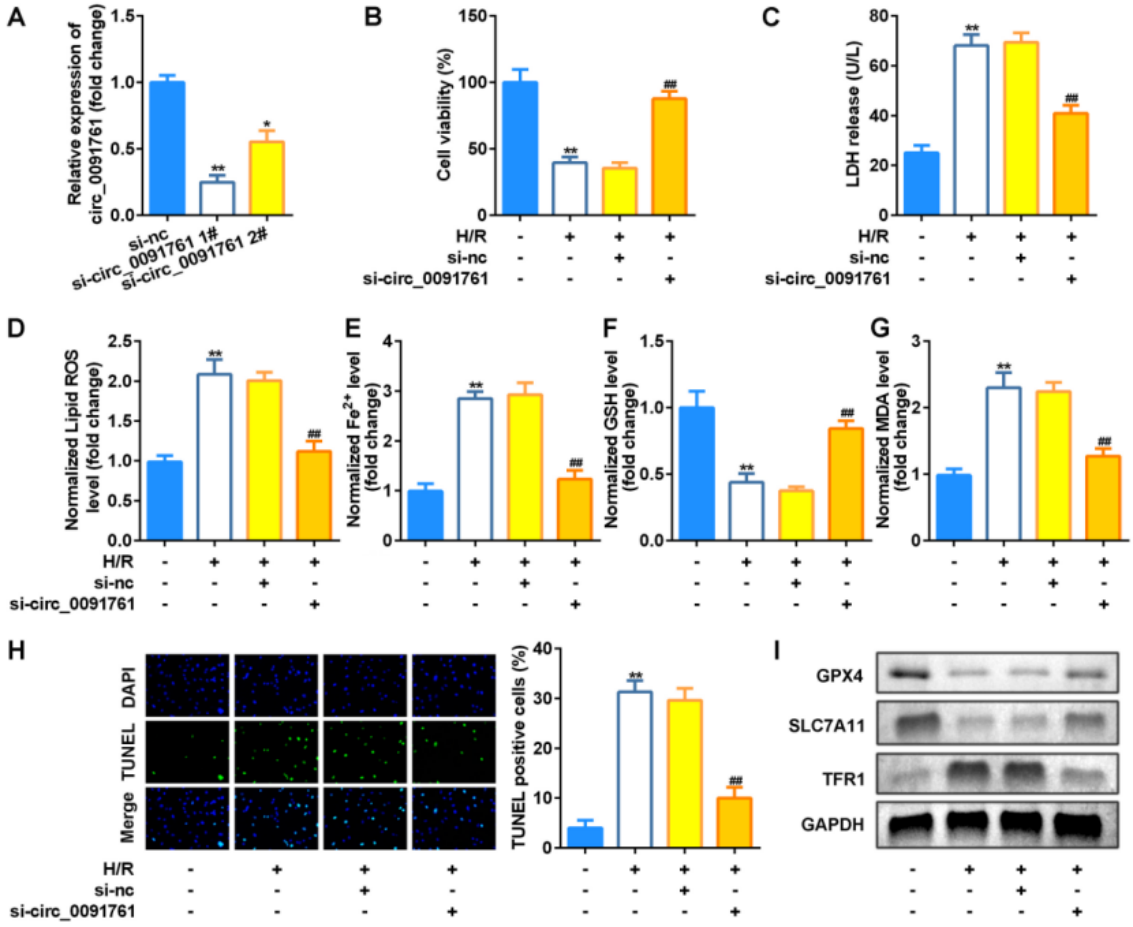

Figure 2. Inhibition of circ_0091761 promoted cell proliferation and inhibited ferroptosis of H/R injured H9c2 cells.
(**A**) Circ_0091761 expression levels were detected by qRT-PCR in H9c2 cells after transfection, $^{*}p<0.05$, $^{**}p<0.01$, compared with the si-na group. (**B**) CCK-8 assay was applied for cell viability detection, $^{**}p<0.01$, compared with the control group; $^{\#\#}p<0.01$, compared with the H/R+ si-NC group. (**C–G**) Levels of LDH, ROS, Fe^{2+}, GSH, and MDA in H/R injured H9c2 cells after transfection, $^{**}p<0.01$, compared with the control group; $^{\#\#}p<0.01$, compared with the H/R+ si-NC group. (**H**) Images and quantized bar chart of TUNEL stained cells, $^{**}p<0.01$, compared with the control group; $^{\#\#}p<0.01$, compared with the H/R+ si-NC group. (**I**) Expression of GPX4, SLC7A11, and TFR1 proteins detected by western blotting.

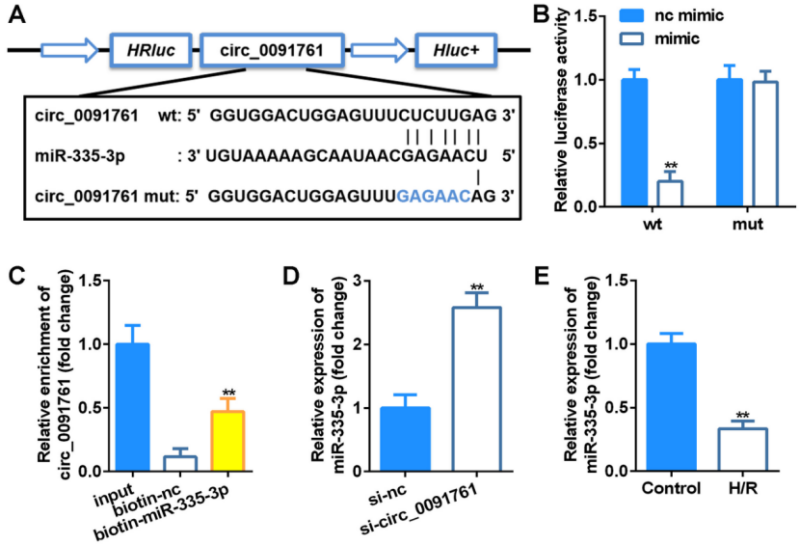

Figure 3. Circ_0091761 served as a miRNA sponge for miR-335-3p
(**A**) The binding sites between miR-335-3p and circ_0091761. (**B**) Luciferase assay of H9c2 cells co-trasfected with mutated miR-335-3p minic and a luciferase vector containing circ_0091761-3′UTR-wt or mutant constructs with mutated miRNA binding sites, $^{**}p<0.01$. (**C**) RNA pull-down assay revealed the enrichment of circ_0091761 on biotin-miR-335-3p, $^{**}p<0.01$, compared with the biotin-NC group. (**D–E**) qRT-PCR analysis for the expression of miR-335-3p, $^{**}p<0.01$.

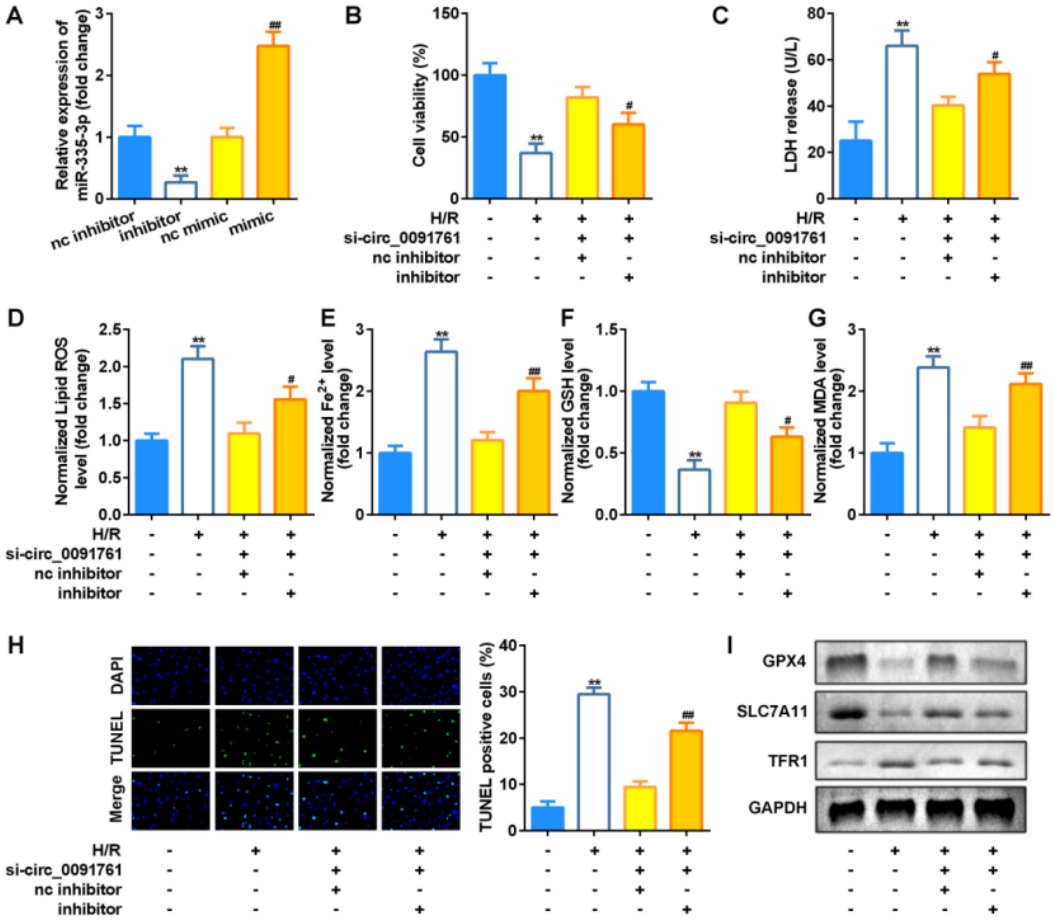

Figure 4. Suppression of miR-335-3p reversed the effects of circ_0091761 on cell proliferation and ferroptosis in H/R injured H9c2 cells.
(**A**) miR-335-3p expression levels were detected by qRT-PCR in H9c2 cells after transfection, $^{**}p<0.01$, compared with the NC inhibitor group; $^{\#\#}p<0.01$, compared with the NC mimic group. (**B**) CCK-8 assay was applied for cell viability detection, $^{**}p<0.01$, compared with the control group; $^{\#\#}p<0.01$, compared with the H/R+ si-circ_0091761+ NC inhibitor group. (**C–G**) Levels of LDH, ROS, Fe^{2+}, GSH, and MDA in H/R injured H9c2 cells after transfection, $^{**}p<0.01$, compared with the control group; $^{\#\#}p<0.01$, compared with the H/R+ si-circ_0091761+ NC inhibitor group. (**H**) Images and quantized bar chart of TUNEL stained cells, $^{**}p<0.01$, compared with the control group; $^{\#\#}p<0.01$, compared with the H/R+ si-circ_0091761+ NC inhibitor group. (**I**) Expression of GPX4, SLC7A11, and TFR1 proteins detected by western blotting.

cell death (Fig. 2H). Simultaneously, LDH, ROS, Fe^{2+}, and MDA concentrations were declined while secretion of GSH was induced after circ_0091761 was silenced (Fig. 2C–G). Furthermore, ferroptosis-related proteins were detected. H/R injury decreased the GPX4 as well as SLC7A11 expression and increased the expression of TFR1, which were reversed by si- circ_0091761 significantly (Fig. 2I).

Circ_0091761 can bind with miR-335-3p

Potential interactions between circRNAs and miRNAs were evaluated using a Circular RNA Interactome online database (https://circinteractome.irp.nia.nih.gov/), and miR-335-3p was expected to bind with circ_0091761 (Fig. 3A). The luciferase activity reporter results demonstrated that luciferase-labeled miR-335-3p mimic and wild-type circ_0091761 co-transfection groups were decreased compared to that of the NC mimic (Fig. 3B). Furthermore, circ_0091761 was primarily enriched in the biotin-miR-335-3p group analyzed by RNA pull-down assay (Fig. 3C). Inhibition of circ_0091761 upregulated the expression of miR-335-3p (Fig. 3D). Furthermore, miR-335-3p was lowly expressed in H/R injured H9c2 cells (Fig. 3E).

Suppression of miR-335-3p reverses the effects of circ_0091761 on cell viability and ferroptosis in H/R injured H9c2 cells

miR-335-3p expression was downregulated by miR-335-3p inhibitor and upregulated by miR-335-3p mimic, suggesting that H/R injured H9c2 cells were successfully transfected (Fig. 4A). miR-335-3p inhibitor obviously switched the effects of si-circ_0091761 on cell proliferation (Fig. 4B) as well as cell death (Fig. 4H). Furthermore, inhibited miR-335-3p alleviated the effects of downregulated circ_0091761 on the secretion of LDH, ROS, Fe^{2+}, MDA, and GSH (Fig. 4C-G) and the expression levels of GPX4, SLC7A11, and TFR1 proteins (Fig. 4I).

miR-335-3p directly targets ACSL4

TargetScan7.2 online database algorithm (http://www.targetscan.org/mmu_72/) was used to predict potential downstream targets of miR-335-3p and we identified ACSL4 as the potential candidate (Fig. 5A). Luciferase activity, as well as RNA pull-down assays further confirmed the binding relationship between miR-335-3p and ACSL4 (Fig. 5B and 5C). Furthermore, ASCL4 expression was negatively regulated by miR-335-3p (Fig. 5D).

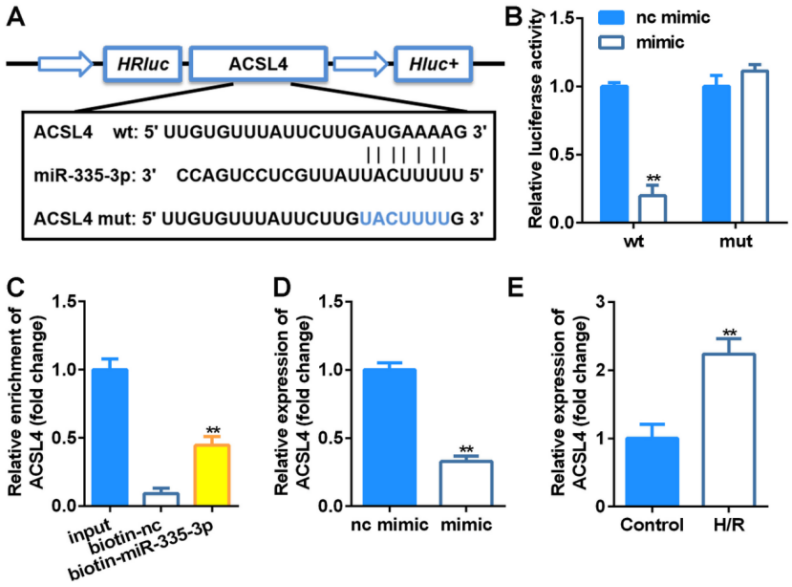

Figure 5. miR-335-3p directly targeted ACSL4.
(**A**) Bioinformatics predicted the binding sites between miR-335-3p and ASCL4. (**B**) Dual-luciferase reporter assay was conducted to confirm the association between ASCL4 and miR-335-3p, $^{**}p<0.01$. (**C**) RNA pull-down assay revealed the enrichment of ASCL4 on biotin-miR-335-3p, $^{**}p<0.01$, compared with the biotin-NC group. (**D–E**) qRT-PCR analysis for the expression of ASCL4, $^{**}p<0.01$.

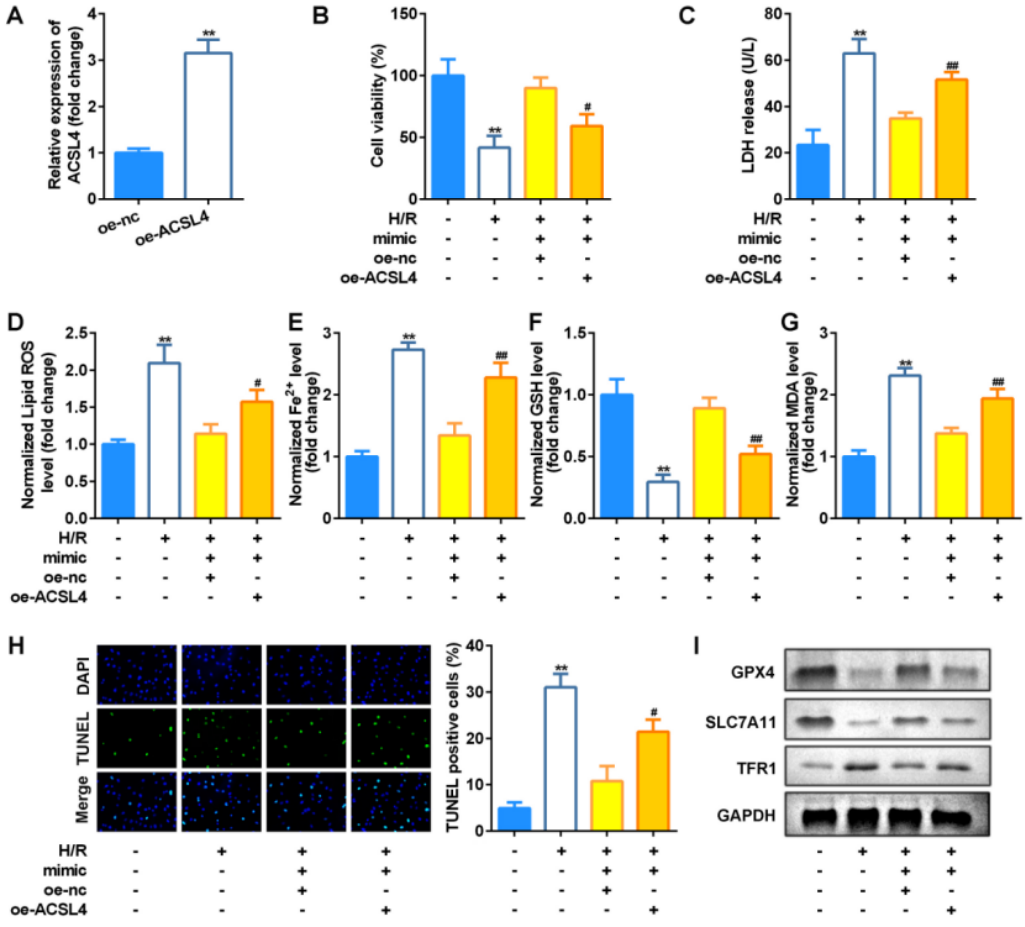

Figure 6. Overexpression of ACSL4 inhibited the effects of upregulated miR-335-3p.
(**A**) ACSL4 expression levels were detected by qRT-PCR in H9c2 cells after transfection, $^{**}p<0.01$. (**B**) CCK-8 assay was applied for cell viability detection, $^{**}p<0.01$, compared with the control group; $^{\#}p<0.05$, compared with the H/R+ mimic+ OE-NC group. (**C–G**) Levels of LDH, ROS, Fe^{2+}, GSH, and MDA in H/R injured H9c2 cells after transfection, $^{**}p<0.01$, compared with the control group; $^{\#}p<0.05$, $^{\#\#}p<0.01$, compared with the H/R+ mimic+ OE-NC group. (**H**) Images and quantized bar chart of TUNEL stained cells, $^{**}p<0.01$, compared with the control group; $^{\#}p<0.05$, compared with the H/R+ mimic+ OE-NC group. (**I**) Expression of GPX4, SLC7A11, and TFR1 proteins detected by western blotting.

Besides, ACSL4 was remarkably highly expressed in H/R injured H9c2 cells (Fig. 5E).

Overexpression of ACSL4 inhibits the effects of upregulated miR-335-3p

As indicated in Fig. 6A, ACSL4 was significantly highly expressed after transfection. Compared with miR-335-3p-overexpressing cells, co-transfection with miR-335-3p and ACSL4 vectors significantly suppressed cell viability (Fig. 6B) and facilitated ferroptosis (Fig. 6C–I).

DISCUSSION

HF is a common complication of MI. MI combined with HF is a clinically acute severe disease with high mortality. There is clinical value in identifying markers that can be obtained early and interpreted easily. Our study suggested that inhibition of circ_0091761 protected HF after MI by upheaving miR-335-3p to inhibit ACSL4 *in vitro*.

Accumulating studies have shown that ferroptosis plays a crucial role in the progression of cardiac dysfunction after MI (Park TJ *et al*., 2019). In the mouse MI model, GPX4 is downregulated and heme oxygenase 1 (Hmox1) is upregulated in myocardial cells to degrade heme and release free iron, leading to mitochondrial dysfunction and ferroptosis. In addition, inhibition of GPX4 transcription in isolated H9c2 cells and neonatal mouse ventricular myocytes resulted in the accumulation of lipid hydroperoxides leading to cell ferroptosis (Park *et al*., 2019, Li *et al*., 2019; Fang *et al*., 2019). These results suggest that ferroptosis is an important pathophysiological change of cardiac function injury after MI. What's more, ferroptosis participates in the occurrence and development of HF (Fang *et al*., 2020; Vegter *et al*., 2016). Inhibiting ferroptosis can reduce cardiomyocyte hypertrophy, improve ventricular dilation, and enhance the function of myocardial dilation and contraction (Fang *et al*., 2020). In vitro cardiomyocytes pretreated with isoproterenol could inhibit the expression of GPX4 and ferritin heavy chain 1, increase the lipid hydroperoxide, and lead to ferroptosis in cardiomyocytes (Park *et al*., 2019; Fang *et al*., 2020). Antagonizing ferroptosis can effectively slow down the process of HF (Fang *et al*., 2019; Friedmann *et al*., 2014; Li *et al*., 2020). Ferroptosis inhibitor can effectively inhibit the increase of free iron and lipid peroxidation in cardiomyocytes and reduce ferroptosis induced by isoproterenol (Fang *et al*., 2019; Zou *et al*., 2020).

Previous studies have shown that the Fenton reaction of ferrous iron in a labile iron pool (LIP) can produce a large number of ROS (Sui *et al*., 2018). When the production of ROS exceeds the compensatory limit of GSH/GPX4, PUFAs containing arachidonic acid and adrenal acid are easily peroxidized and accumulated by ROS, leading to ferroptosis in cells (Yang *et al*., 2016). In other words, GSH/GPX4 can inhibit lipid peroxidation in the cell membrane, thus inhibiting ferroptosis in cells. However, a large amount of studies have discovered new pathways that inhibit cell iron death during GSH/GPX4 inactivation. It was found that the N-terminus of Ferrastatin-1 was mystoacylated to promote the recruitment of coenzyme Q10 to the cell membrane, reducing it to a reduced coenzyme, and inhibiting ferroptosis in cells (Bersuker *et al*., 2019). The antagonistic effect of FSP1 on ferroptosis was independent of GSH/GPX4 (Doll *et al*., 2019). In addition, the metabolites of guanosine triphosphate hydrolase 1 (GCH-1), tetrahydrobiopterin and dihydrobiopterin (BH4/BH2), can selectively inhibit the peroxidation of membrane polyunsaturated fatty acids containing two acyl-tail, and GCH1 can promote the production of coenzyme Q10 and inhibit cell ferroptosis in collaboration with FSP1 (Kraft *et al*., 2020). These studies also found a range of genes that suppress lipid peroxidation in the absence of GPX4, providing new directions for future research. At present, the research on the regulation factors of iron death is still insufficient and needs further exploration.

Circ_0091761 is a newfound circRNA with a sliced length of 709bp, located on the X chromosome. Zhao *et al* collected blood samples of coronary arteries of MI patients as well as healthy controls, the intersection results of multiple bioinformatics analysis data showed that 4 dysregulated circRNAs (circRNA_0001654, circRNA_0091761, circRNA_0405624, and circRNA_0406698) may be associated with the regulation of MI process (Zhao *et al*., 2020). In the present research, our data suggested that circRNA_0091761 was the highest expressed circRNA identified in H/R injured H9c2 cells, and was further elevated by ferroptosis inducer RSL3 whereas downregulated by ferroptosis inhibitor Ferrastatin-1, suggesting that upregulation of circ_0091761 may be associated with ferroptosis in H/R injured H9c2 cells. Subsequently, inhibition of circ_0091761 promoted cell viability and suppressed ferroptosis of H/R injured H9c2 cells, demonstrating that circ_0091761 may protect against HF after MI by suppressing ferroptosis *in vitro*, which was in line with previous studies (Fang *et al*., 2020).

Recently, various studies have reported that miRNAs play essential roles in cardiovascular diseases (Vegter *et al*., 2016). For instance, the downregulation of miR-221-3p and miR-222-3p promoted myocardial fibrosis of HF (Verjans *et al*., 2018). In MI studies, miRNA-21 treatment of cardiomyocytes and endothelial cells significantly suppressed apoptosis and significantly improved cardiac function (Song *et al*., 2019). In this study, we hypothesized that circRNA_0091761 might bind certain miRNAs to regulate HF after MI. Our data indicated that miR-335-3p has a specific binding effect with circRNA_0091761. Further functional experiments confirmed that miR-335-3p inhibitor could effectively reduce the proliferation promotion and ferroptosis inhibition effects of suppressed circrNA_0091761 on H/R injured H9c2 cells. All results confirmed that circRNA_0091761 can regulate the expression of related genes by binding miR-335-3p and play a role in inhibiting ferroptosis and thus HF progression.

ACSL4 drives ferroptosis by oxidizing cell membrane phospholipids, whichhave been recognized to be a typical marker of ferroptosis (Doll *et al*., 2017; Song *et al*., 2019). The ectonucleotide pyrophosphatase-phosphodiesterase 2 (ENPP2)/ lysophosphatidic acid (LPA) protected myocardial cells from erastin induced ferroptosis by regulating the expression of GPX4, ACSL4 and Nrf2 (Bai *et al*., 2018). Our finding demonstrated that ACSL4 was a downstream gene of miR-335-3p, and overexpression ACSL4 obviously revealed miR-335-3p mimicked induced effects on cell viability as well as ferroptosis. Thence, on the basis of these findings, we concluded that circ_0091761 promoted ferroptosis in H/R injured H9c2 cells via binding with miR-335-3p to upregulate ACSL4.

CONCLUSION

The findings of the present study indicated that circ_0091761 functioned as a ceRNA to regulate ACSL4 expression by sponging miR-335-3p to regulate HF after the MI process *in vitro*. Therefore, inhibition of

circ_0091761 may be a potential target for protection against HF after MI.

Declarations

Funding. Not applicable.

Conflict of Interests. The authors confirm that no conflicts of interest exist in this work.

Acknowledgments. Not applicable.

Ethical approval. No ethics approval was required for this study as it involved no human participants or animals.

REFERENCES

Altesha MA, Ni T, Khan A, Liu K, Zheng X (2019) Circular RNA in cardiovascular disease. *J Cell Physiol* **234**: 5588–5600. https://doi.org/10.1002/jcp.27384

Ashwal-Fluss R, Meyer M, Pamudurti NR, Ivanov A, Bartok O, Hanan M, Evantal N, Memczak S, Rajewsky N, Kadener S (2014) circRNA biogenesis competes with pre-mRNA splicing. *Mol Cell* **56:** 55–66. https://doi.org/10.1016/j.molcel.2014.08.019

Bahit MC, Kochar A, Granger CB (2018) Post-myocardial infarction heart failure. *JACC Heart Fail* **6**: 179–186. https://doi.org/10.1016/j.jchf.2017.09.015

Bai YT, Chang R, Wang H, Xiao FJ, Ge RL, Wang LS (2018) ENPP2 protects cardiomyocytes from erastin-induced ferroptosis. *Biochem Biophys Res Commun* **499**: 44–51. https://doi.org/10.1016/j.bbrc.2018.03.113

Bersuker K, Hendricks JM, Li Z, Magtanong L, Ford B, Tang PH, Roberts MA, Tong B, Maimone TJ, Zoncu R, Bassik MC, Nomura DK, Dixon SJ, Olzmann JA (2019) The CoQ oxidoreductase FSP1 acts parallel to GPX4 to inhibit ferroptosis. *Nature* **575**: 688–692. https://doi.org/10.1038/s41586-019-1705-2

Cao JY, Dixon SJ (2016) Mechanisms of ferroptosis. *Cell Mol Life Sci* **73**: 2195–209. https://doi.org/10.1007/s00018-016-2194-1

Devaux Y, Creemers EE, Boon RA, Werfel S, Thum T, Engelhardt S, Dimmeler S, Squire I (2017) Cardiolinc network. Circular RNAs in heart failure. *Eur J Heart Fail* **19**: 701–709. https://doi.org/10.1002/ejhf.801

Doll S, Freitas FP, Shah R, Aldrovandi M, da Silva MC, Ingold I, Goya Grocin A, Xavier da Silva TN, Panzilius E, Scheel CH, Mourão A, Buday K, Sato M, Wanninger J, Vignane T, Mohana V, Rehberg M, Flatley A, Schepers A, Kurz A, White D, Sauer M, Sattler M, Tate EW, Schmitz W, Schulze A, O'Donnell V, Proneth B, Popowicz GM, Pratt DA, Angeli JPF, Conrad M (2019) FSP1 is a glutathione-independent ferroptosis suppressor. *Nature* **575**: 693–698. https://doi.org/10.1038/s41586-019-1707-0

Doll S, Proneth B, Tyurina YY, Panzilius E, Kobayashi S, Ingold I, Irmler M, Beckers J, Aichler M, Walch A, Prokisch H, Trümbach D, Mao G, Qu F, Bayir H, Füllekrug J, Scheel CH, Wurst W, Schick JA, Kagan VE, Angeli JP, Conrad M (2017) ACSL4 dictates ferroptosis sensitivity by shaping cellular lipid composition. *Nat Chem Biol* **13**: 91–98. https://doi.org/10.1038/nchembio.2239. **13(1)**:91-8

Fang X, Cai Z, Wang H, Han D, Cheng Q, Zhang P, Gao F, Yu Y, Song Z, Wu Q, An P, Huang S, Pan J, Chen HZ, Chen J, Linkermann A, Min J, Wang F (2020) Loss of cardiac ferritin h facilitates cardiomyopathy *via* Slc7a11-mediated ferroptosis. *Circ Res* **127**: 486–501. https://doi.org/10.1161/CIRCRESAHA.120.316509

Fang X, Wang H, Han D, Xie E, Yang X, Wei J, Gu S, Gao F, Zhu N, Yin X, Cheng Q, Zhang P, Dai W, Chen J, Yang F, Yang HT, Linkermann A, Gu W, Min J, Wang F (2019) Ferroptosis as a target for protection against cardiomyopathy. *Proc Natl Acad Sci U S A* **116**: 2672–2680. https://doi.org/10.1073/pnas.1821022116

Friedmann Angeli JP, Schneider M, Proneth B, Tyurina YY, Tyurin VA, Hammond VJ, Herbach N, Aichler M, Walch A, Eggenhofer E, Basavarajappa D, Rådmark O, Kobayashi S, Seibt T, Beck H, Neff F, Esposito I, Wanke R, Förster H, Yefremova O, Heinrichmeyer M, Bornkamm GW, Geissler EK, Thomas SB, Stockwell BR, O'Donnell VB, Kagan VE, Schick JA, Conrad M (2014) Inactivation of the ferroptosis regulator Gpx4 triggers acute renal failure in mice. *Nat Cell Biol* **16**: 1180–1191. https://doi.org/10.1038/ncb3064

Hu H, Chen Y, Jing L, Zhai C, Shen L (2021) The link between ferroptosis and cardiovascular diseases: a novel target for treatment. *Front Cardiovasc Med* **8**: 710963. https://doi.org/10.3389/fcvm.2021.710963

Kraft VAN, Bezjian CT, Pfeiffer S, Ringelstetter L, Müller C, Zandkarimi F, Merl-Pham J, Bao X, Anastasov N, Kössl J, Brandner S, Daniels JD, Schmitt-Kopplin P, Hauck SM, Stockwell BR, Hadian K, Schick JA (2020) GTP Cyclohydrolase 1/tetrahydrobiopterin counteract ferroptosis through lipid remodeling. *ACS Cent Sci* **6**: 41–53. https://doi.org/10.1021/acscentsci.9b01063

Li M, Duan L, Li Y, Liu B (2019) Long noncoding RNA/circular noncoding RNA-miRNA-mRNA axes in cardiovascular diseases. *Life Sci* **233**: 116440. https://doi.org/10.1016/j.lfs.2019.04.066

Li W, Feng G, Gauthier JM, Lokshina I, Higashikubo R, Evans S, Liu X, Hassan A, Tanaka S, Cicka M, Hsiao HM, Ruiz-Perez D, Bredemeyer A, Gross RW, Mann DL, Tyurina YY, Gelman AE, Kagan VE, Linkermann A, Lavine KJ, Kreisel D (2019) Ferroptotic cell death and TLR4/Trif signaling initiate neutrophil recruitment after heart transplantation. *J Clin Invest* **129**: 2293–2304. https://doi.org/10.1172/JCI126428

Li Y, Cao Y, Xiao J, Shang J, Tan Q, Ping F, Huang W, Wu F, Zhang H, Zhang X (2020) Inhibitor of apoptosis-stimulating protein of p53 inhibits ferroptosis and alleviates intestinal ischemia/reperfusion-induced acute lung injury. *Cell Death Differ* **27**: 2635–2650. https://doi.org/10.1038/s41418-020-0528-x

Meng S, Zhou H, Feng Z, Xu Z, Tang Y, Li P, Wu M (2017) CircRNA: functions and properties of a novel potential biomarker for cancer. *Mol Cancer* **16**: 94. https://doi.org/10.1186/s12943-017-0663-2

Orrem HL, Nilsson PH, Pischke SE, Grindheim G, Garred P, Seljeflot I, Husebye T, Aukrust P, Yndestad A, Andersen GØ, Barratt-Due A, Mollnes TE (2018) Acute heart failure following myocardial infarction: complement activation correlates with the severity of heart failure in patients developing cardiogenic shock. *ESC Heart Fail* **5**: 292–301. https://doi.org/10.1002/ehf2.12266

Park TJ, Park JH, Lee GS, Lee JY, Shin JH, Kim MW, Kim YS, Kim JY, Oh KJ, Han BS, Kim WK, Ahn Y, Moon JH, Song J, Bae KH, Kim DH, Lee EW, Lee SC (2019) Quantitative proteomic analyses reveal that GPX4 downregulation during myocardial infarction contributes to ferroptosis in cardiomyocytes. *Cell Death Dis* **10**: 835. https://doi.org/10.1038/s41419-019-2061-8

Si X, Zheng H, Wei G, Li M, Li W, Wang H, Guo H, Sun J, Li C, Zhong S, Liao W, Liao Y, Huang S, Bin J (2020) circRNA Hipk3 induces cardiac regeneration after myocardial infarction in mice by binding to Notch1 and miR-133a. *Mol Ther Nucleic Acids* **21**: 636–655. https://doi.org/10.1016/j.omtn.2020.06.024

Song Y, Zhang C, Zhang J, Jiao Z, Dong N, Wang G, Wang Z, Wang L (2019) Localized injection of miRNA-21-enriched extracellular vesicles effectively restores cardiac function after myocardial infarction. *Theranostics* **9**: 2346–2360. https://doi.org/10.7150/thno.29945

Song Y, Zhang C, Zhang J, Jiao Z, Dong N, Wang G, Wang Z, Wang L (2019) Localized injection of miRNA-21-enriched extracellular vesicles effectively restores cardiac function after myocardial infarction. *Theranostics* **9**: 2346–2360. https://doi.org/10.7150/thno.29945

Sui X, Zhang R, Liu S, Duan T, Zhai L, Zhang M, Han X, Xiang Y, Huang X, Lin H, Xie T (2018) RSL3 drives ferroptosis through GPX4 inactivation and ROS production in colorectal cancer. *Front Pharmacol* **9**: 1371. https://doi.org/10.3389/fphar.2018.01371

Vegter EL, van der Meer P, de Windt LJ, Pinto YM, Voors AA (2016) MicroRNAs in heart failure: from biomarker to target for therapy. *Eur J Heart Fail* **18**: 457–468. https://doi.org/10.1002/ejhf.495

Verjans R, Peters T, Beaumont FJ, van Leeuwen R, van Herwaarden T, Verhesen W, Munts C, Bijnen M, Henkens M, Diez J, de Windt LJ, van Nieuwenhoven FA, van Bilsen M, Goumans MJ, Heymans S, González A, Schroen B (2018) MicroRNA-221/222 family counteracts myocardial fibrosis in pressure overload-induced heart failure. *Hypertension* **71**: 280–288. https://doi.org/10.1161/HYPERTENSIONAHA.117.10094

Xiao MS, Wilusz JE (2019) An improved method for circular RNA purification using RNase R that efficiently removes linear RNAs containing G-quadruplexes or structured 3' ends. *Nucleic Acids Res* **47**: 8755–8769. https://doi.org/10.1093/nar/gkz576

Xie Y, Hou W, Song X, Yu Y, Huang J, Sun X, Kang R, Tang D (2016) Ferroptosis: process and function. *Cell Death Differ* **23**: 369–379. https://doi.org/10.1038/cdd.2015.158

Yang WS, Kim KJ, Gaschler MM, Patel M, Shchepinov MS, Stockwell BR (2016) Peroxidation of polyunsaturated fatty acids by lipoxygenases drives ferroptosis. *Proc Natl Acad Sci U S A.* **113(34)**:E4966-75. https://doi.org/10.1073/pnas.1603244113

Zhang Y, Liang W, Zhang P, Chen J, Qian H, Zhang X, Xu W (2017) Circular RNAs: emerging cancer biomarkers and targets. *J Exp Clin Cancer Res* **36**: 152. https://doi.org/10.1186/s13046-017-0624-z

Zhao C, Liu J, Ge W, Li Z, Lv M, Feng Y, Liu X, Liu B, Zhang Y (2021) Identification of regulatory circRNAs involved in the pathogenesis of acute myocardial infarction. *Front Genet* **11**: 626492. https://doi.org/10.3389/fgene.2020.626492

Zou Y, Henry WS, Ricq EL, Graham ET, Phadnis VV, Maretich P, Paradkar S, Boehnke N, Deik AA, Reinhardt F, Eaton JK, Ferguson B, Wang W, Fairman J, Keys HR, Dančík V, Clish CB, Clemons PA, Hammond PT, Boyer LA, Weinberg RA, Schreiber SL (2020) Plasticity of ether lipids promotes ferroptosis susceptibility and evasion. *Nature* **585**: 603–608. https://doi.org/10.1038/s41586-020-2732-8